Evaluating Combinations of Optimizers and Loss Functions for Cloud Removal Using Diffusion Models

Leandro Henrique Furtado Pinto Silva[1,2], João Fernando Mari[1], Mauricio C. Escarpinati[2]
and André R. Backes[3]
[1] *Institute of Exact and Technological Sciences, Federal University of Viçosa - UFV, Rio Paranaíba-MG, Brazil*
[2] *School of Computer Science, Federal University of Uberlândia, Uberlândia, Brazil*
[3] *Department of Computing, Federal University of São Carlos, São Carlos-SP, Brazil*
{leandro.furtado, joaof.mari}@ufv.br, mauricio@ufu.br, arbackes@yahoo.com.br

Keywords: Cloud Removal, Diffusion Model, Remote Sensing, Optimizers, Loss Functions.

Abstract: Cloud removal is crucial for photogrammetry applications, including urban planning, precision agriculture, and climate monitoring. Recently, generative models, especially those based on latent diffusion, have shown remarkable results in high-quality synthetic image generation, making them suitable for cloud removal tasks. These approaches require optimizing numerous trainable parameters with various optimizers and loss functions. This study evaluates the impact of combining three optimizers (SGD, Adam, and AdamW) with the MAE, MSE, and Huber loss functions. For evaluation, we used the SEN_MTC_New dataset, which contains pairs of 4-band images with and without clouds, divided into training, validation, and test sets. The results, measured in terms of PSNR and SSIM, show that the diffusion model combining AdamW and the Huber loss function delivers exceptional performance in cloud removal.

1 INTRODUCTION

Remote sensing, particularly through satellite imagery, is vital for environmental monitoring, urban planning, and precision agriculture. However, these applications are significantly hindered by cloud presence, as clouds can obscure areas of interest, affecting measurement accuracy (Jeppesen et al., 2019; Arakaki et al., 2023; Ferreira et al., 2024). This issue is especially impactful given that clouds with various characteristics cover approximately 60% of the Earth's surface and continuously shift across regions. Consequently, cloud removal techniques to reduce these artifacts have gained prominence in recent research (Xie et al., 2023; Podsiadlo et al., 2020).

To address cloud removal, researchers have employed various approaches, including Convolutional Neural Networks (CNNs), Generative Adversarial Networks (GANs), and, more recently, Diffusion Models (Dong et al., 2021). Although each method has unique attributes, they are united by their reliance on deep learning, and tuning these models often involves empirical considerations (Barbosa et al., 2024). Choosing the right optimizers and loss functions is essential to improving the learning process by accurately updating model weights, which supports better generalization (Seyrek and Uysal, 2024). Notably, while optimizer and loss function choices are crucial for traditional Convolutional Neural Networks, these elements require further investigation for emerging techniques like latent diffusion models.

Through analysis of nine experiments, this study examines which combinations of optimizers and loss functions yield optimal results for cloud removal. Our investigation focuses on the performance impact of these combinations in diffusion models for cloud removal tasks.

The remaining of this work is organized as follows: Section 2 presents related works, providing definitions that support and motivate this study. Section 3 details the Materials and Methods, including the experimental setup, dataset, and evaluation metrics. Section 4 presents the quantitative and qualitative results and discussions. Finally, Section 5 presents the conclusions, perspectives of this research, and future works.

2 RELATED WORKS

The work by Zhao and Jia (2023) introduces a sequence-based diffusion model for generating cloud-

Silva, L. H. F. P., Mari, J. F., Escarpinati, M. C. and Backes, A. R.
Evaluating Combinations of Optimizers and Loss Functions for Cloud Removal Using Diffusion Models.
DOI: 10.5220/0013252100003912

In *Proceedings of the 20th International Joint Conference on Computer Vision, Imaging and Computer Graphics Theory and Applications (VISIGRAPP 2025) - Volume 3: VISAPP*, pages 648-656
ISBN: 978-989-758-728-3; ISSN: 2184-4321

free images. This model employs multimodal diffusion for training and sequential inference, integrating multi-temporal information in a time-invariant manner. Experiments conducted on the four bands of the public SEN12MS-CR-TS dataset demonstrated that this model outperforms other approaches in the literature, highlighting its flexibility in processing sequences of arbitrary length.

Zhao et al. (2023) propose a CNN-based method that takes advantage of radio frequency signals in the ultra-high and super-high frequency bands, allowing it to "see" through clouds to assist in image reconstruction. This innovative multimodal and multitemporal approach demonstrated effectiveness in producing cloud-free images in experiments with public satellite data.

Ebel et al. (2023) present UnCRtainTS, a multitemporal cloud removal method that combines attention-based features with specialized architectures to predict multivariate uncertainties. Experiments conducted on two public datasets showed this approach's high effectiveness in reconstructing images obscured by clouds.

The study by Wang et al. (2023) introduces a cloud removal algorithm based on (i) time-series reference imagery, (ii) selection of similar pixels through weighted temporal and spectral distances, and (iii) residual image estimation. The algorithm creates two "buffer zones" around clouded areas, enabling automatic selection of an "optimal" set of time-series reference images. Experiments across four diverse locations, such as urban, rural, and humid areas, which demonstrated the model's quantitative effectiveness, adaptability to varying cloud sizes, and superior performance compared to other methods, with efficient computational time that makes it suitable for large datasets.

3 MATERIAL AND METHODS

3.1 Image Dataset

For our experiments, we used the multitemporal SEN2_MTC_New dataset, a heterogeneous collection of images from various Earth regions (Huang and Wu, 2022). This dataset consists of 50 tiles, each divided into 256×256 patches across four bands: Red, Green, Blue, and Near Infrared, including both thin and thick cloud coverage. Areas with thin clouds contain more land information, which is crucial for the reconstruction process; however, thin clouds pose challenges in cloud segmentation, potentially impacting cloud removal accuracy. In contrast, thick clouds simplify segmentation, but the land information is more limited in these images.

The dataset contains $2,380$ image patches for training, 350 for validation, and 687 for testing, with each patch containing pairs of cloud-covered images and their corresponding cloud-free counterparts. For our experiments, we considered the same quantity as the original dataset. Figure 1 shows samples of the patches in the dataset.

3.2 DiffCR

Zou et al. (2024) introduced DiffCR, a diffusion model for cloud removal that generates Gaussian noise from cloud-free images and uses this noise to produce new synthetic cloudless images for a given cloudy input image. This Gaussian noise represents a latent space where encoding and decoding occur through a U-Net architecture (Ronneberger et al., 2015). A key innovation in DiffCR is the integration of the Time and Condition Fusion Block (TCF-Block) in place of traditional transformer mechanisms used in latent diffusion models. TCFBlock reduces computational costs and enhances the model's performance on cloud removal tasks by improving the visual correspondence between the generated image and the ground truth.

DiffCR comprises three main components: (i) the condition encoder, (ii) the time encoder, and (iii) the denoising autoencoder. The condition and time encoders extract spatial and multiscale features from clouded images and incorporate temporal features based on noise levels from the diffusion model. These features then guide the denoising autoencoder, aiding in the gradual reduction of noise to create clear images. The authors emphasize that the choice of loss function is essential in directing the generation of realistic, cloud-free synthetic images, a motivation that also supports this research.

3.3 Optimizers

Due to the complexity of deep learning models, especially with regard to the large number of trainable parameters, optimizers play a crucial role in the learning process. In general terms, optimizers iteratively adjust model weights, helping guide the model toward an efficient and optimal solution (Ruder, 2017).

Stochastic Gradient Descent (SGD) (Robbins and Monro, 1951) is an optimization algorithm that updates weights by moving in the opposite direction of the loss function's gradient. In general terms, Equation 1 defines SGD weights update:

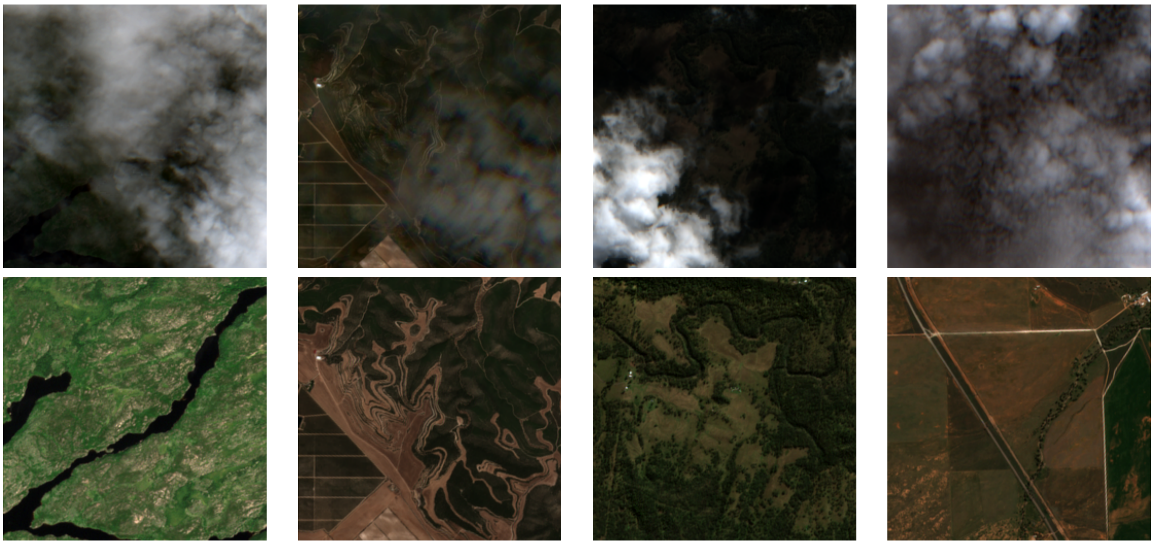

Figure 1: Samples of SEN2_MTC_New dataset. The first row shows images with clouds, and the second shows the corresponding cloudless images.

$$\theta_{t+1} = \theta_t - \eta \nabla_\theta J(\theta_t), \tag{1}$$

where η is the learning rate, θ are the weights, and $\nabla_\theta J(\theta_t)$ is the gradient for updating the weights.

Momentum is an essential hyperparameter for SGD, as it helps reduce large oscillations and accelerates training convergence. In general terms, momentum accumulates past gradients to smooth the weight updates. This accumulation of gradients (v_t) to momentum is defined according to Equation 2:

$$v_t = \gamma v_{t-1} + \eta \nabla_\theta J(\theta_t), \tag{2}$$

where γ assigns the contribution of the previous gradient (v_{t-1}).

Thus, with the use of Momentum, the SGD is defined according to Equation 3:

$$\theta_{t+1} = \theta_t - v_t, \tag{3}$$

Adam Kingma (2014) is an optimizer that combines elements of both RMSProp and Momentum. Specifically, it tracks an average of past gradients as well as a mean of the squares of these gradients, enabling more adaptive weight updates.

Thus, the following are stored respectively: (i) exponential mean of the gradients (m_t) and (ii) exponential mean of the squares of the gradients (s_t), as defined by Equations 4 and 5:

$$m_t = \beta_1 m_{t-1} + (1 - \beta_1) \nabla_\theta J(\theta_t), \tag{4}$$

$$s_t = \beta_2 s_{t-1} + (1 - \beta_2)(\nabla_\theta J(\theta_t))^2, \tag{5}$$

where β_1 and β_2 are the exponential decay factors.

Thus, the update of the weights in Adam occurs according to Equations 6 and 7:

$$\hat{m}_t = \frac{m_t}{1 - \beta_1^t}, \quad \hat{s}_t = \frac{s_t}{1 - \beta_2^t}, \tag{6}$$

$$\theta_{t+1} = \theta_t - \eta \frac{\hat{m}_t}{\sqrt{\hat{s}_t} + \varepsilon}, \tag{7}$$

where ε is a small value to avoid zero division.

The AdamW optimizer (Loshchilov and Hutter, 2019) adapts Adam, which inserts weight decay directly into the weight update. For AdamW, the storage components are the same as those in Adam: an average of past gradients and a mean of the gradients' squares (Equations 4 and 5). Thus, the update of the weights of AdamW is defined according to Equation 8.

$$\theta_{t+1} = \theta_t - \eta \left(\frac{m_t}{\sqrt{v_t} + \varepsilon} + \lambda \theta_t \right), \tag{8}$$

where λ is the weight decay factor.

3.4 Loss Function

Loss functions play a key role in model training by guiding the updates of weights and gradients. In our experiments, we used the Mean Squared Error (MSE), Mean Absolute Error (MAE), and Huber loss functions, employing their default settings in PyTorch [1].

MAE calculates the absolute difference between the predicted and actual values (ground truth), while

[1] https://pytorch.org/docs/stable/nn.html#loss-functions

MSE calculates the square of this difference. These relationships are shown in Equations 9 and 10:

$$\text{MAE} = \frac{1}{N}\sum_{i=1}^{N}|x_i - y_i|, \tag{9}$$

$$\text{MSE} = \frac{1}{N}\sum_{i=1}^{N}(x_i - y_i)^2, \tag{10}$$

where x_i is the predicted pixel value; y_i is the the expected pixel value; and N is the number of pixels in an image.

The Huber loss function combines aspects of MAE and MSE, depending on a specified value of δ. It penalizes larger errors more heavily while smoothing smaller errors, as defined in Equation 11:

$$\text{Huber} = \begin{cases} 0.5 \cdot (x_i - y_i)^2, & \text{if } |x_i - y_i| < \delta \\ \delta \cdot (|x_i - y_i| - 0.5 \cdot \delta), & \text{otherwise} \end{cases} \tag{11}$$

For our experiments, as with Pytorch's default configuration, we used $\delta = 1.0$.

3.5 Experimental Setup

We conducted nine experimental setups using the DiffCR baseline[2]. For model training, we tested three optimizers: AdamW, Adam, and SGD. We also evaluated three loss functions: Huber, MSE, and MAE. In all experiments, we used a learning rate of 5×10^{-5}, a weight decay of 0.01 to mitigate overfitting, and a batch size of 16. It is important to note that weight decay affects each optimizer differently and directly influences weight update dynamics. For instance, weight decay impacts only the weights in AdamW, whereas in SGD and Adam, it also affects the gradient. For SGD, we additionally used a momentum of 0.9.

Training was conducted for $3,000$ epochs, with validation occurring every 200 epochs to monitor learning progress in each experiment, using validation losses based on MAE, MSE, and Huber functions. Additionally, we set a seed of 42 for all experiments to ensure reproducibility. Figure 2 summarizes the experimental design of this study.

3.6 Evaluation Metrics

The Structural Similarity Index Measure (SSIM) consists of a metric used to evaluate the quality of an image using a reference image. We considered a Gaussian filter with a standard deviation of 1.0 for this index. The SSIM metric is defined according to Equation 12

$$\text{SSIM}(x,y) = \frac{(2\mu_x\mu_y + C_1)(2\sigma_{xy} + C_2)}{(\mu_x^2 + \mu_y^2 + C_1)(\sigma_x^2 + \sigma_y^2 + C_2)}, \tag{12}$$

where x and y are two patches obtained from respective images to be evaluated. Values of x and y are defined as non-negative values representing a signal, which must be aligned; μ_x is the pixel sample mean of signal x; μ_y is the pixel sample mean of signal y; σ_x^2 is the variance of signal x; σ_y^2 is the variance of signal y; σ_{xy} is the covariance of signals x and y; C_1 and C_2 are two constants included to avoid instability to values very close to zero.

The Peak signal-to-noise ratio (PSNR) is another metric for evaluating distortion between images. The PSNR is defined in terms of MSE acording to Equation 13

$$\text{PSNR} = 10\log_{10}\left(\frac{255^2}{\text{MSE}}\right) \tag{13}$$

3.7 Computational Environment

The experiments were performed on a PC with a 4.4 GHz Core i5-12400 CPU and 32 GB of RAM. The PC has an NVIDIA RTX 4090 GPU (24 GB memory). The experiments used Python 3.10.14 programming language and NumPy and Matplotlib libraries for numerical processing and visualization of images and data. The Scikit-learn library was used to manipulate the set of images and analyze the classification results. The library used to implement the deep neural network models was PyTorch 2.3.1 and CUDA 12.1.

4 RESULTS

Validation is a crucial step in monitoring a model's learning process to understand its behavior, avoid overfitting, and make targeted adjustments. In this study, we evaluated validation loss for all experiments using the MAE, MSE, and Huber loss functions, as shown in Figure 3. The figure indicates that the model overfits only in the configuration of SGD + MAE loss. For the other configurations, a reduction in validation loss suggests effective learning. Validation also reveals that the model performs better with the Adam and AdamW optimizers across all loss functions, particularly AdamW, which exhibits less severe oscillations.

We assessed the trained models on the full SEN2_MTC_New test set using PSNR and SSIM metrics. Table 1 consolidates these results, showing

[2] https://xavierjiezou.github.io/DiffCR/

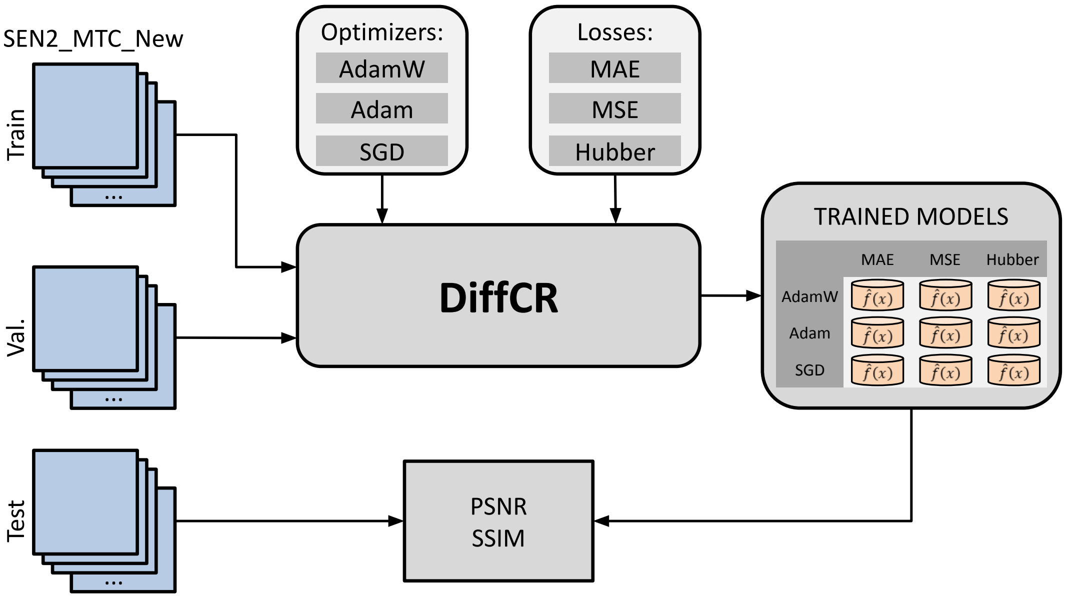

Figure 2: Experimental design of this work.

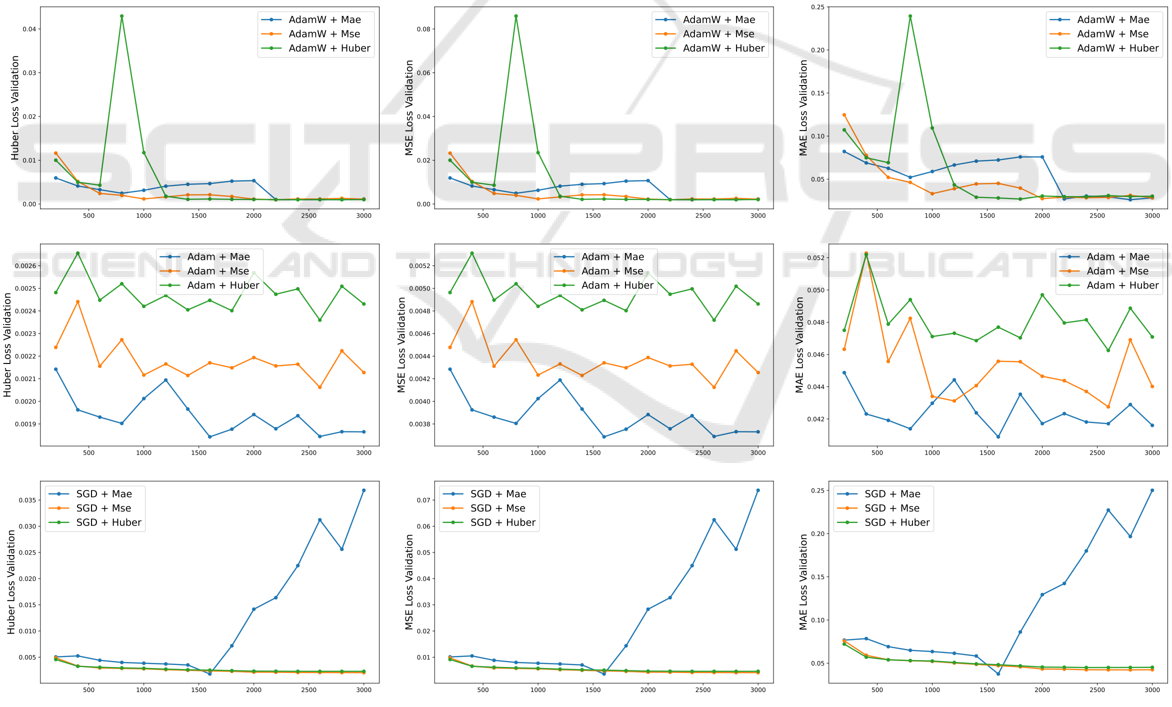

(a) **(b)** **(c)**

Figure 3: Model Validation every 200 epochs. Columns (a), (b), and (c) present the validation in terms of Huber Loss Validation, MSE Loss Validation, and MAE Loss Validation, respectively. Each row represents the AdamW, Adam, and SGD optimizers, respectively, with each optimizer having three training loss functions.

the mean, standard deviation, and maximum value achieved by each model for both metrics. Figures 4 and 5 further illustrate these results visually.

Overall, the best results were obtained with the AdamW optimizer. This optimizer generally provides a stable PSNR and SSIM across the three loss functions. However, while the mean values for PSNR remain close (around 17–18 dB) for MAE and MSE losses, the Huber loss shows a slight increase in SSIM (0.5871) and a significantly higher maximum PSNR

(32.3323). The Huber function's selective penalization of larger errors may have contributed to the superior performance, as it avoids uniform penalization regardless of error magnitude. This configuration effectively addresses cloud removal in images containing varied contexts (e.g., rivers, forests, urban areas) and diverse cloud types and densities, treating areas with heavier cloud cover more stringently to produce realistic images. Additionaly, these results may indicate that the Huber loss can better handle noisy or outlier data, which could explain the significant increase in PSNR.

In the experiments with the Adam optimizer, the differences between loss functions are relatively minor. While there is some variation, no configuration offers a significant performance boost. This implies that Adam might not benefit as much from tuning the loss function in this application, offering limited flexibility for improvement without switching optimizers. Unlike AdamW, however, the worst overall result was recorded with Huber Loss, while the best was achieved with MAE Loss, suggesting that Adam might introduce more abrupt updates during training. This optimizer generally achieves lower PSNR and SSIM values across all loss functions when compared to AdamW. This suggests that Adam may not be as effective for optimizing these image quality metrics, potentially due to the optimizer's sensitivity to hyperparameter settings.

Finally, for the SGD optimizer, both MSE and Huber losses offer a more stable and moderate performance for PSNR and SSIM, except for the overfitted SGD + MAE model. Given the dataset's heterogeneous nature, we observed substantial standard deviations across all experiments, which underscores the challenges posed by diverse land covers. SGD with MAE loss yields the lowest average PSNR (5.3825 ± 3.2556) and a significantly lower SSIM (0.1996 ± 0.0944), indicating instability or poor convergence in this combination. However, the maximum PSNR achieved (17.8467) suggests that this combination can sometimes produce reasonable outputs, although it's inconsistent. Further research into hyperparameter tuning could help improve performance in such varied contexts, refining the model to reduce deviations and enhance diffusion model generalization.

For qualitative evaluation, Figures 6 and 7 present results from two image patches (with corresponding cloudy and cloudless references) across all experiments. These figures show how the results align with the quantitative findings. The examples represent different land cover types, cloud densities, and shadowing, highlighting challenges such as shadowed regions and heavy cloud cover. Figure 6 depicts a highly clouded area with minimal visible ground information, while Figure 7 shows a less clouded region with prominent shadows. Across all experiments, handling shadowed areas remains a consistent challenge, akin to the difficulty observed with thick clouds. The "AdamW + Huber" combination achieves a visual result that closely matches the expected outcome, with the most notable differences occurring in areas of denser cloud cover. Other combinations exhibit various reconstruction issues, including loss of information that was originally visible and unobstructed by clouds. Additionally, other optimizer combinations struggle to accurately reconstruct aspects of the image, such as tonality and texture, even in visible regions, with "SGD + MAE" failing to generate a coherent image.

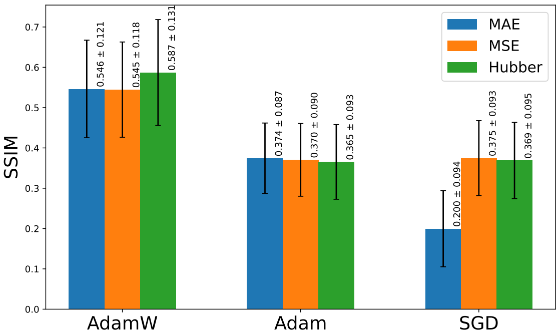

Figure 4: Visualization and comparison of SSIM metric results in the test set for each model.

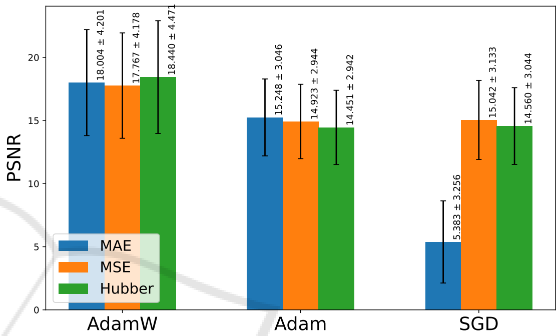

Figure 5: Visualization and comparison of PSNR metric results in the test set for each model.

5 CONCLUSIONS

The selection of an optimizer and cost function has a significant impact on training latent diffusion models. For the cloud removal task, this study demonstrated that these choices directly affect model performance, either enhancing or hindering results.

Table 1: Experimental Results for Test Set.

Optimizer	Loss	PSNR ↑	SSIM ↑	Max PSNR	Max SSIM
AdamW	MAE	18.0040 ± 4.2008	0.5463 ± 0.1210	28.4146	0.8115
	MSE	17.7674 ± 4.1784	0.5447 ± 0.1181	27.8317	0.8433
	Huber	18.4395 ± 4.4706	0.5871 ± 0.1313	32.3323	0.8903
Adam	MAE	15.2478 ± 3.0464	0.3745 ± 0.0873	22.6487	0.6597
	MSE	14.9229 ± 2.9440	0.3704 ± 0.0902	21.0076	0.6169
	Huber	14.4507 ± 2.9423	0.3653 ± 0.0926	20.0854	0.6143
SGD	MAE	5.3825 ± 3.2556	0.1996 ± 0.0944	17.8467	0.6674
	MSE	15.0421 ± 3.1325	0.3748 ± 0.0929	21.1497	0.6193
	Huber	14.5604 ± 3.0442	0.3688 ± 0.0946	20.2948	0.6237

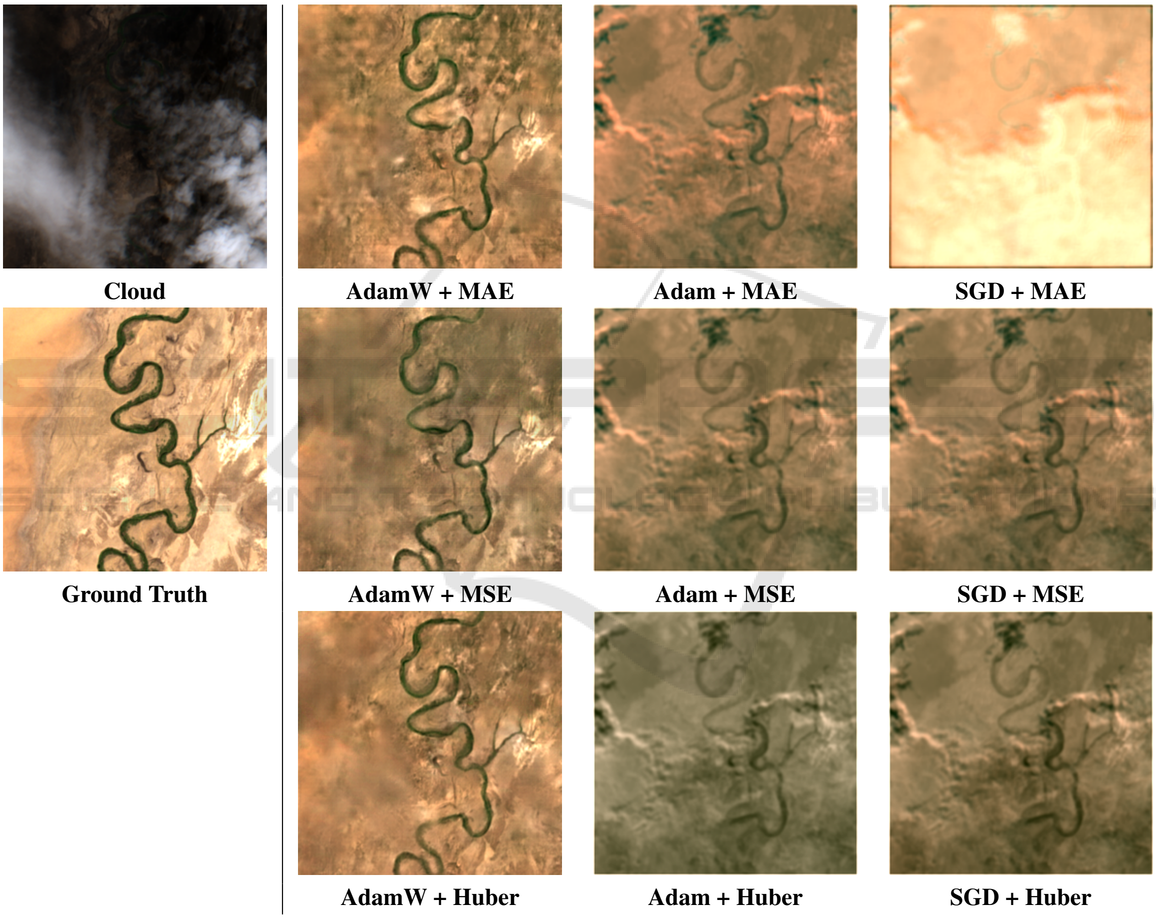

Figure 6: Qualitative results of our experiments. The first column presents one of three multitemporal patches with clouds and respective Ground Truth (cloudless). The other patches present visualizations of each of the nine experiments of this work.

In particular, the combination of the Huber function with the AdamW optimizer proved effective for cloud removal, given the complex nature of the problem, which involves varying cloud types, ground cover, and shadows, each posing unique local challenges for reconstruction. AdamW facilitated smoother training, while the Huber loss function effectively emphasized regions with higher cloud occlusion, preserving areas that were already cloud-free.

For future work, we plan to explore alternatives to the TCFBlock from the DiffCR baseline, broaden the hyperparameter search space (e.g., learning rate and weight decay), and implement an early stopping strategy.

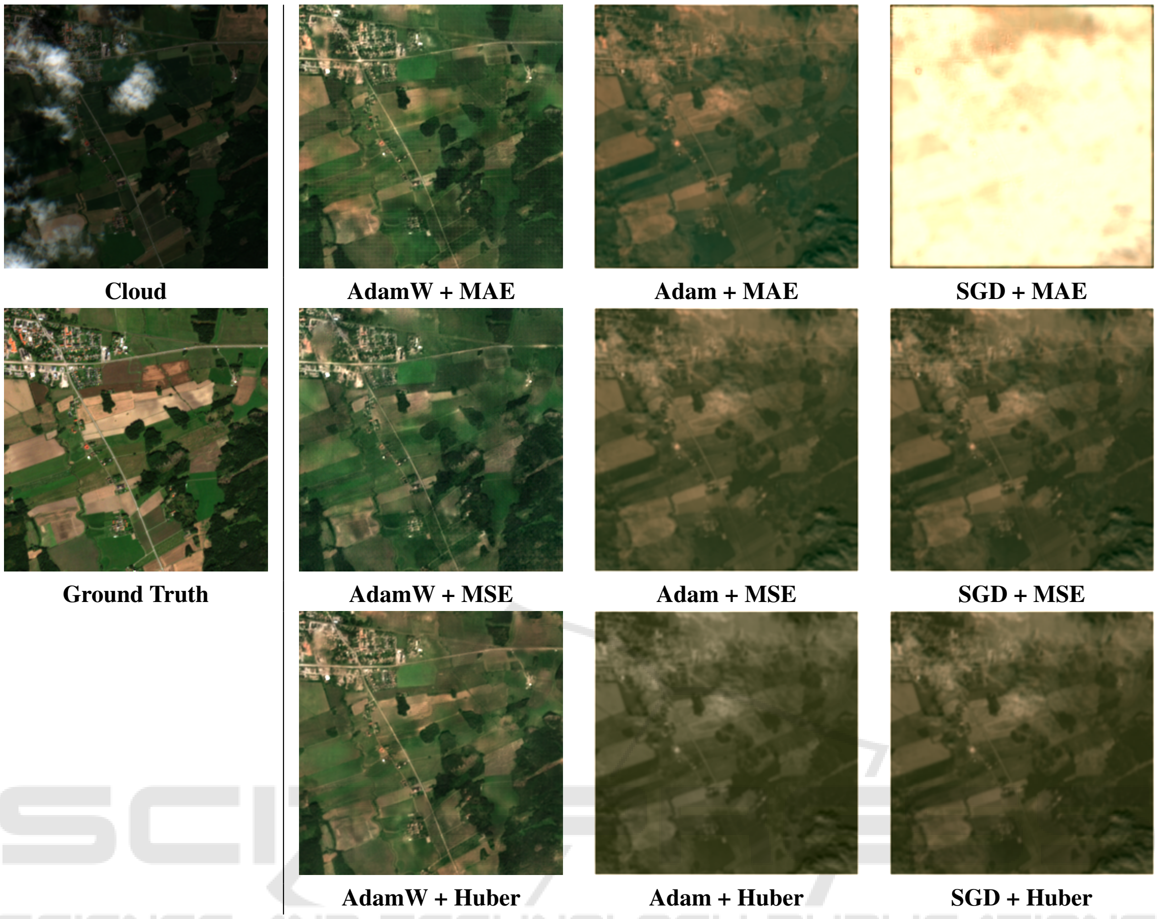

Figure 7: Qualitative results of our experiments. The first column presents one of three multitemporal patches with clouds and respective Ground Truth (cloudless). The other patches present visualizations of each of the nine experiments of this work.

ACKNOWLEDGEMENTS

We would like to thank FAPEMIG, Brazil (Grant number CEX - APQ-02964-17) for financial support. André R. Backes gratefully acknowledges the financial support of CNPq (National Council for Scientific and Technological Development, Brazil) (Grant #307100/2021-9). This study was financed in part by the Coordenação de Aperfeiçoamento de Pessoal de Nível Superior - Brazil (CAPES) - Finance Code 001.

REFERENCES

Arakaki, L. G., Silva, L. H. F. P., da Silva, M. V., Melo, B. M., Backes, A. R., Escarpinati, M. C., and Mari, J. F. (2023). Evaluation of u-net backbones for cloud segmentation in satellite images. In *Proceedings of the 18th International Joint Conference on Computer Vision, Imaging and Computer Graphics Theory and Applications (VISIGRAPP 2023) - Volume 4: VISAPP*, pages 452–458. INSTICC, SciTePress.

Barbosa, G., Moreira, L., de Sousa, P. M., Moreira, R., and Backes, A. (2024). Optimization and learning rate influence on breast cancer image classification. In *Proceedings of the 19th International Joint Conference on Computer Vision, Imaging and Computer Graphics Theory and Applications - Volume 3: VISAPP*, pages 792–799. INSTICC, SciTePress.

Dong, S., Wang, P., and Abbas, K. (2021). A survey on deep learning and its applications. *Computer Science Review*, 40:100379.

Ebel, P., Garnot, V. S. F., Schmitt, M., Wegner, J. D., and Zhu, X. X. (2023). Uncrtaints: Uncertainty quantification for cloud removal in optical satellite time series. In *Proceedings of the IEEE/CVF Conference on Computer Vision and Pattern Recognition*, pages 2085–2095.

Ferreira, J. R., Silva, L. H. F. P., Escarpinati, M. C., Backes, A. R., and Mari, J. F. (2024). Evaluating multiple combinations of models and encoders to segment clouds in satellite images. In *Proceedings of the 19th*

International Joint Conference on Computer Vision, Imaging and Computer Graphics Theory and Applications - Volume 3: VISAPP, pages 233–241. INSTICC, SciTePress.

Huang, G.-L. and Wu, P.-Y. (2022). Ctgan: Cloud transformer generative adversarial network. In *2022 IEEE International Conference on Image Processing (ICIP)*, pages 511–515. IEEE.

Jeppesen, J. H., Jacobsen, R. H., Inceoglu, F., and Toftegaard, T. S. (2019). A cloud detection algorithm for satellite imagery based on deep learning. *Remote sensing of environment*, 229:247–259.

Kingma, D. P. (2014). Adam: A method for stochastic optimization. *arXiv preprint arXiv:1412.6980*.

Loshchilov, I. and Hutter, F. (2019). Decoupled weight decay regularization.

Podsiadlo, I., Paris, C., and Bruzzone, L. (2020). A study of the robustness of the long short-term memory classifier to cloudy time series of multispectral images. In *Image and Signal Processing for Remote Sensing XXVI*, volume 11533, pages 335–343. SPIE.

Robbins, H. and Monro, S. (1951). A stochastic approximation method. *The annals of mathematical statistics*, pages 400–407.

Ronneberger, O., Fischer, P., and Brox, T. (2015). U-net: Convolutional networks for biomedical image segmentation.

Ruder, S. (2017). An overview of gradient descent optimization algorithms.

Seyrek, E. C. and Uysal, M. (2024). A comparative analysis of various activation functions and optimizers in a convolutional neural network for hyperspectral image classification. *Multimedia Tools and Applications*, 83(18):53785–53816.

Wang, Z., Zhou, D., Li, X., Zhu, L., Gong, H., and Ke, Y. (2023). Virtual image-based cloud removal for landsat images. *GIScience & Remote Sensing*, 60(1):2160411.

Xie, Y., Li, Z., Bao, H., Jia, X., Xu, D., Zhou, X., and Skakun, S. (2023). Auto-cm: Unsupervised deep learning for satellite imagery composition and cloud masking using spatio-temporal dynamics. In *Proceedings of the AAAI Conference on Artificial Intelligence*, volume 37, pages 14575–14583.

Zhao, M., Olsen, P., and Chandra, R. (2023). Seeing through clouds in satellite images. *IEEE Transactions on Geoscience and Remote Sensing*, 61:1–16.

Zhao, X. and Jia, K. (2023). Cloud removal in remote sensing using sequential-based diffusion models. *Remote Sensing*, 15(11):2861.

Zou, X., Li, K., Xing, J., Zhang, Y., Wang, S., Jin, L., and Tao, P. (2024). Diffcr: A fast conditional diffusion framework for cloud removal from optical satellite images. *IEEE Transactions on Geoscience and Remote Sensing*, 62:1–14.